Available online at www.ijournalse.org

Emerging Science Journal

(ISSN: 2610-9182)

Vol. 8, No. 3, June, 2024

Performance Optimization of Step-Like Divergence Plenum Air-Cooled Li-Ion Battery Thermal Management System Using Variable-Step-Height Configuration

Olanrewaju M. Oyewola [1*], Adetokunbo A. Awonusi [2], Olawale S. Ismail [2]

[1] *Department of Mechanical Engineering, University of Alaska Fairbanks, Alaska, United States.*

[2] *Department of Mechanical Engineering, University of Ibadan, Ibadan, Nigeria.*

Abstract

Several studies on air-cooled battery thermal management systems (BTMSs) have shown that improvement can be achieved through redesign of the BTMSs. Recent studies have achieved improvements in managing the temperature in the system, but mostly with an increase in pressure drop. It is therefore imperative to carry out an extended study or redesign of the existing designs to overcome these challenges. In this work, a standard Z-type BTMS, which has a flat divergence plenum, was redesigned to have a step-like divergence plenum of variable step height. Computational Fluid Dynamics (CFD) approach was adopted to investigate the thermal and airflow performance of the BTMSs. The CFD methodology was validated by comparing its results with experimental data in the literature. Various step height configurations were considered for 3-step and 4-step models. Findings from the result revealed that the variable step height design enhances the cooling performance of the battery pack. For instance, a 3-step model with step heights of 3, 6, and 6 mm offered the least pressure drop and maximum temperature difference, and when compared with the model with a constant step height of 5, 5, and 5 mm, it yielded reductions of 3.4% and 21.6%, respectively. By increasing the inlet airflow velocity, the 4-step cases generally improved. The best cooling improvement was seen in case 26 at velocities over 3.7 m/s for maximum temperature and velocities over 4.8 m/s for maximum temperature difference.

Keywords:

Step-Like Plenum;
Step Height;
Optimization;
BTMS.

Article History:

Received:	08	February	2024
Revised:	11	May	2024
Accepted:	18	May	2024
Published:	01	June	2024

1- Introduction

In recent years, electric vehicles (EVs) have gained increased popularity as a substitute for fossil fuel-driven vehicles in the transportation sector due to the massive release of harmful pollutants such as carbon dioxide by fossil fuel-driven vehicles, which has adverse effects on the environment. One important component of the EV is the battery pack, whose performance has a significant impact on the vehicle's power output, mileage, and market pricing [1]. While the battery pack is in operation, a significant amount of heat is produced, which could result in an extremely high battery temperature and a wide variation in temperature among the batteries in the pack. These problems affect the battery's performance and can reduce its lifespan. Lithium-ion batteries are one of the most frequently utilized batteries for EVs because of their great capacity and efficiency. The battery operates best at a temperature between 25 and 40 °C [2], and the battery pack's temperature gradient should not be more than 5 °C [3]. Hence, a battery thermal management system (BTMS) that will provide an optimal battery temperature and keep a steady temperature distribution inside the battery pack is required. In that regard, the research and development of BTMS made use of

* **CONTACT**: oooyewola001@gmail.com; ooyewola@alaska.edu

DOI: http://dx.doi.org/10.28991/ESJ-2024-08-03-01

different cooling technologies, such as heat pipe cooling [4, 5], liquid cooling [6–8], phase change material (PCM) cooling [9, 10], and air cooling [11–15]. When considering the cost of production, operation, and maintenance, air-cooling technologies are the best and more preferred technology globally. However, due to the low specific heat of the air, it becomes vulnerable to large temperature variations and high temperatures inside the battery packs. Hence, researchers made several attempts to improve the air-cooled BTMS's cooling performance, either by adding more components, redesigning its structure, or a combination of the two.

Some researchers looked into the effects of the BTMS's inlet and outlet positions [13–18], while others investigated number of inlet and outlets [18–21]. For instance, Chen et al. [13] studied BTMSs with various outlet and inlet positions. It was discovered that the symmetrical BTMS with an outlet and inlet in the middle of the plenums yielded improved thermal performance. When the optimized BTMS was compared to the standard Z-type BTMS, the maximum temperature (T_{max}) and maximum temperature differential (ΔT_{max}) decreased by 4.5 K and 7.7 K, respectively. In another study, Jiaqiang et al. [16] investigated several air-cooling techniques by using a baffle and varying the distance between the BTMS inlet and outlet. The study reported that by positioning the air flow inlet and outlet locations on different sides of the module, and using baffles, optimum performance of the BTMS was attained. The size and position of the secondary vent's effect on BTMS performance were investigated by Hong et al. [18]. Findings from the study indicated that secondary vent's position has a significant impact on the battery pack's T_{max} and ΔT_{max}. Shahid & Agelin-Chaab [19] used an input plenum as a supplementary inlet with axial airflow in a passive battery pack to enhance temperature uniformity. By evaluating the battery pack's cooling efficiency against a baseline scenario, the average $T_{max}$of batteries reduced by 4% and temperature homogeneity increased by 39%. Zhang et al. [20] further examined the effect of number and size of baffles and secondary outlets on BTMS cooling capacity. Based on the findings from the study, the T_{max} and ΔT_{max} were minimized after optimization and when compared to the conventional Z-type BTMS, reduced by 1.84°C and 3.66°C, respectively. The cooling channel was also equipped with a baffle according to the initial optimization model, and it was found that when compared with standard Z-type BTMS, T_{max} and ΔT_{max}were reduced by 4.49 °C and 2.17 °C, respectively.

Other researchers focused on battery spacing distribution [22–24] and battery cell architecture [25, 26]. In a study by Fan et al. [25], a battery system with 32 cylindrical lithium-ion batteries arranged across, laterally, and vertically was investigated. The layout with the best thermal homogeneity and performance was shown to be aligned, then staggered, and finally cross-shaped. The alignment configuration consumed around 23% less energy than the cross arrangement. Similarly, Peng et al. [26] examined the effects of various battery configurations, air intake and outlet locations, as well as the number of outlets and inlets, on a BTMS. They observed that a moderate length-to-width ratio is preferable for improving cooling system performance. Chen et al. [22] modified battery spacing, which was reported to have improved the thermal performance air-cooled BTMS. The study further adopted an optimization approach, which was reported to have significantly improved the performance of the system, resulting in a 42% decrease in the T_{max} and a slight decrease in ΔT_{max} without increase in the total pressure difference in the system. In another study, battery module with 36 lithium-ion cells, was analyzed by Li et al. [23]. From the analyses, it was discovered that increasing the overall mass flow rate may cause the profile of the channel mass flow to be more uneven and that a large channel spacing size may worsen temperature stability on the battery walls. Also, when the system's cooling channel size was optimized, the T_{max} was reduced from 23.9 K to 2.1 K and the ΔT_{max} from 25.7 K to 6.4 K.

Several studies also investigated effect of the inclination of the plenum on the performance BTMS [27-30]. In the study by Chen et al. [25], inlet air temperature and flow rate, and battery pack C-discharge rate were investigated. After optimizing the system, it was found that the cooling performance of the BTMS was significantly improved, resulting in a 42% decrease in the T_{max} and a slight decrease in ΔT_{max}without increase in the total pressure difference of the system. Similarly, Oyewola et al. [28] investigated the effects of inlet and outlet plenum angles of standard Z and U-type flow BTMS to optimize the flow and thermal distribution in the systems. The results demonstrated that by adjusting the inlet plenum angle to 150° and the outlet plenum angle to 120°, the performance of standard Z-type flow cooling improved. T_{max} reduced by 1.6 °C, the ΔT_{max}reduced by 3.7 °C, and the power consumption reduced by 29%. The standard U-type flow BTMS's cooling efficiency also improved by keeping the outlet plenum angle at 135° and leaving the inlet plenum angle perpendicular. The power consumption reduced by 11%, the T_{max} reduced by 0.4 °C, and the ΔT_{max} reduced by 1 °C.

In addition to changing the air-cooling BTMS structure, researchers also attempted to install additional materials such as plates [31, 32], heat sinks [33, 34], spoilers [35, 36], and baffles [16, 20] to alter the airflow distribution. Zhang et al. [36] added spoilers to the airflow path of the inlet plenum to enhance its cooling efficiency. The effects of spoiler quantity and placement on the thermal behavior of a BTMS were examined. The T_{max} and ΔT_{max} were decreased by 1.86 K and 2.51 K, respectively, when compared with the original model. The effects of parallel plate height and length on the thermal efficiency of the BTMS were examined by Wang et al. [17]. The plates were placed parallel along the system's cooling channels. Results show that the cooling module with a pair of parallel plates exhibited excellent thermal performance within the allowable power consumption loss range. Also, the impacts of the parallel plate's height and length were examined, with the optimal values being 1.5 mm and 30 mm, respectively.

In order to further improve the cooling performance of existing BTMSs, researchers now adopt the combination of two existing cooling strategies, known as hybrid cooling strategies (HCS), to optimize the performance of the designs with a single cooling strategy [37–40]. For instance, Mousavi et al. [37] adopted a hybrid design that combines phase change material (PCM) and mini-channel cold plates (MCPs). The study reported that the maximum temperature in the battery pack was reduced by 30 K in the optimum system. Additionally, under multiple pulsed heat generation, the difference in averages of maximum temperature was less than 1 K between the two cooling systems. In another study, Yang et al. [38] proposed a hybrid battery thermal management system that provides a compact, lightweight, and energy-efficient solution. The results show that the optimum hybrid cold plate design, which only weighs half of the baseline cold plate, can provide more than 50% reduction in the total pumping power while achieving the same cooling performance. More so, Zare et al. [39] developed a new hybrid thermal management system that combines the use of fins and PCM to enhance the performance of the system. The performance of the hybrid BTMS was better when compared to the system with natural air cooling and the PCM cooling system without fins. After the PCM complete melting process, the BTMS with 4 internal-external fins reduced the temperature of the batteries by 9.90 and 17.45 K compared to the PCM cooling system without fins at discharge rates of 3C and 5C, respectively. In order to further enhance the use of hybrid cooling strategies, Khan et al. [40] experimentally studied a hybrid li-ion battery thermal management system with eutectic PCM-embedded heat transfer fluid. The eutectic PCM comprises stearic acid and lauric acid, with a melting temperature of 33.29 °C, a thermal conductivity of 0.356 W/mK, and a latent heat of 151.76 J/g. Experimental results show that with natural air cooling, the maximum temperatures of the battery packs reach 66.9 °C, 57.9 °C, and 45.6 °C when charging and discharging at 2°C, 1.5°C, and 1°C rates, respectively. Furthermore, when compared to natural air cooling at the 2C rate, heat transfer fluid cooling reduced the maximum temperature by 22.42%, eutectic PCM cooling by 40.90%, and hybrid cooling by 46.18%.

Aside from the benefits derived from the HCSs, some researchers are also looking into further optimizing existing single cooling strategy designs, which could later be combined with other designs to further enhance performance of already existing HCSs [41-45]. Shen et al. [44] developed a new BTMS by modifying the Z-shaped conventional design, which was investigated to analyze its thermal performance. By comparing the modified system with the conventional Z-shape the maximum temperature of the battery pack was reduced from 38.15 °C to 34.14 °C, which implies a decrease of 10.5%, while the temperature difference was reduced from 2.59 °C to 1.97 °C, which implies a decrease of 23.9%, In the same vein, Oyewola and Idowu [45] installed steps to the divergence plenum of four flow pattern BTMSs. The results revealed that only one of the designs with step installed; yielded improvement, with maximum temperature and maximum temperature difference reduced by 3.2 K and 7.6 K, respectively when compared to the design without step installed. Additionally, Alzwayi & Paul [41] designed a spiral and vertical fin which was used to enhance the performance of thermal performance of the system by reducing the maximum temperature of batteries. Effects of the fin's number, thickness, rotation, length, and position were investigated at various current rates. The orientation of the fin also has a significantly impact on the heat transfer between the cell and air cooling, with the cell temperature rising by 1.5 °C when compared to the half-length of a longitudinal fin. Furthermore, compared to the longitudinal fins, the spiral fins reduce the cell temperature by 3.2%, resulting in a 65.6% reduction in material usage. Chen et al. [42] developed a control strategy for efficient battery thermal management of an air-cooled system. The control strategy of the BTMS is based on the difference in temperature among the batteries, proposed as the J-type flow. The results with high current discharge rate and varying random operating conditions revealed that the developed system ensured the temperature difference was maintained below 0.5 K after several switches of flow type. The average temperature difference among the batteries in the developed system was reduced by more than 67% when compared to J-type flow alone. In another study, Fini et al. [43] experimentally investigated the effect of pressure on the performance of PCM in li-ion battery thermal management system. The results revealed that at discharge of 7 C, the cell was able to discharge for almost twice as long when subjected to the pressure of 500 kPa when compared to under atmospheric pressure. It was further reported that by increasing the pressure from 100 to 500 kPa increased the depth of discharge by almost 10 %, while doubling the extracted energy.

Aside from the benefits derived from HCSs, some researchers are also looking into further optimizing existing single cooling strategy designs, which could later be combined with other designs to further enhance the performance of already existing HCSs [41–45]. Shen et al. [44] developed a new BTMS by modifying the Z-shaped conventional design, which was investigated to analyze its thermal performance. By comparing the modified system with the conventional Z-shape, the maximum temperature of the battery pack was reduced from 38.15 °C to 34.14 °C, which implies a decrease of 10.5%, while the temperature difference was reduced from 2.59 °C to 1.97 °C, which implies a decrease of 23.9%. In the same vein, Oyewola & Idowu [45] installed steps to the divergence plenum of four flow pattern BTMSs. The results revealed that only one of the designs with a step installed yielded an improvement, with the maximum temperature and maximum temperature difference reduced by 3.2 K and 7.6 K, respectively, when compared to the design without a step installed. Additionally, Alzwayi & Paul [41] designed a spiral and vertical fin that was used to enhance the performance

of thermal performance of the system by reducing the maximum temperature of the batteries. The effects of the fin's number, thickness, rotation, length, and position were investigated at various current rates. The orientation of the fin also has a significant impact on the heat transfer between the cell and air cooling, with the cell temperature rising by 1.5 °C when compared to the half-length of a longitudinal fin. Furthermore, compared to the longitudinal fins, the spiral fins reduce the cell temperature by 3.2%, resulting in a 65.6% reduction in material usage. Chen et al. [42] developed a control strategy for efficient battery thermal management in an air-cooled system. The control strategy of the BTMS is based on the difference in temperature among the batteries, proposed as the J-type flow. The results with a high current discharge rate and varying random operating conditions revealed that the developed system ensured the temperature difference was maintained below 0.5 K after several switches of flow type. The average temperature difference among the batteries in the developed system was reduced by more than 67% when compared to J-type flow alone. In another study, Fini et al. [43] experimentally investigated the effect of pressure on the performance of PCM in a li-ion battery thermal management system. The results revealed that at discharge of 7 °C, the cell was able to discharge for almost twice as long when subjected to a pressure of 500 kPa when compared to under atmospheric pressure. It was further reported that increasing the pressure from 100 to 500 kPa increased the depth of discharge by almost 10% while doubling the extracted energy.

Different cooling strategies are being developed by researchers in recent years to widen the adaptation and application of BTMS. Tian et al. [46] carried out the design and experimental study of wave-type micro-channel cooling plates for large-capacity marine battery thermal management. The study reported that the designed system with non-linear wave-type microchannel could relief the contradiction between cooling capacity and the temperature uniformity. For all the working conditions, the system could maintain the maximum temperature and temperature standard deviation of batteries below 41.5 °C and 0.96 °C, respectively. Also, Zhang et al. [20] optimized the cooling performance of air-cooling lithium-ion battery thermal management system by adopting multiple secondary outlets and baffle. Findings from the study showed that, when compared with the conventional Z-type BTMS, the maximum temperature (T_{max}) and maximum temperature difference (ΔT_{max}) were reduced by 1.84 °C (4.20%) and 3.66 °C (75%) after optimization, respectively. By further introducing a baffle in the cooling channel, the performance of the system was enhanced, and when compared with the conventional Z-type BTMS, the optimized T_{max} and ΔT_{max} were reduced by 2.17 °C (4.95%) and 4.49 °C (91.89%), respectively. Furthermore, Weragoda et al. [47] conceptualized a new BTMS based on capillary-driven evaporative cooling. In the design, a structure was directly integrated onto the battery's surface to enable direct cooling. Experimental study was carried out by affixing a copper foam to an emulated battery block, and using ethanol and Novec 7000 as the cooling media. Findings from the study revealed that copper foam with higher pore density performed better than the others due to its greater wetting height. More so, the maximum battery surface temperature was maintained around 40 °C for a continuous 50W heat input.

According to the aforementioned literatures, the main factor influencing T_{max} and $\Delta T_{max}$of a battery pack is uneven airflow distribution. Hence, by modifying the plenum design of the BTMS, the airflow distribution in the system can be altered, thereby enhancing the cooling efficiency of the BTMS. Consequently, several researches redesigned the divergence plenum of Z-type air-cooled BTMS. One of the new designs is the step-like divergence plenum, developed by Oyewola et al. [48]. The step-like BTMS was reported to significantly improve cooling efficiency, when compared with the conventional Z-type BTMS. However, the study reported that improvement in the cooling efficiency is often accompanied with increase in pressure drop (i.e. increase in power consumption). In this study, the scope of research on existing step-like divergence plenum design of Z-type BTMS [48], with equal height of steps was extended, by varying the height of steps, with the aim of minimizing both the ΔT_{max} and ΔP . Variable step heights optimization was employed and additional studies were carried out to minimize the pressure drop while still achieving reasonable cooling efficiency in terms of maximum temperature in the battery pack. Furthermore, under different inlet flow velocities, the behaviors of each selected case's performance were examined. It is expected that findings from this study will advance system sustainability by providing different concepts of constructing efficient air-cooled BTMS in the future. In summary, the structure of the article comprises; abstract, introduction, methodology, result and discussion, conclusion, and references.

2- Research Methodology

2-1- Physical Geometry

A Z-type air-cooled BTMS system was considered for investigation in this study and depicted in Figure 1. The air and cell properties were obtained from Chen et al. [13] and presented in Table 1. The BTMS consists of nine cooling channels and eight prismatic cells. Each cooling channel has a thickness, d, set to 3 mm, while the dimensions of each battery (length × width × height) are 27 × 70 × 90 mm. For this study, an inlet air temperature and velocity of 299.15 K and 3.5 m/s, respectively, were used.

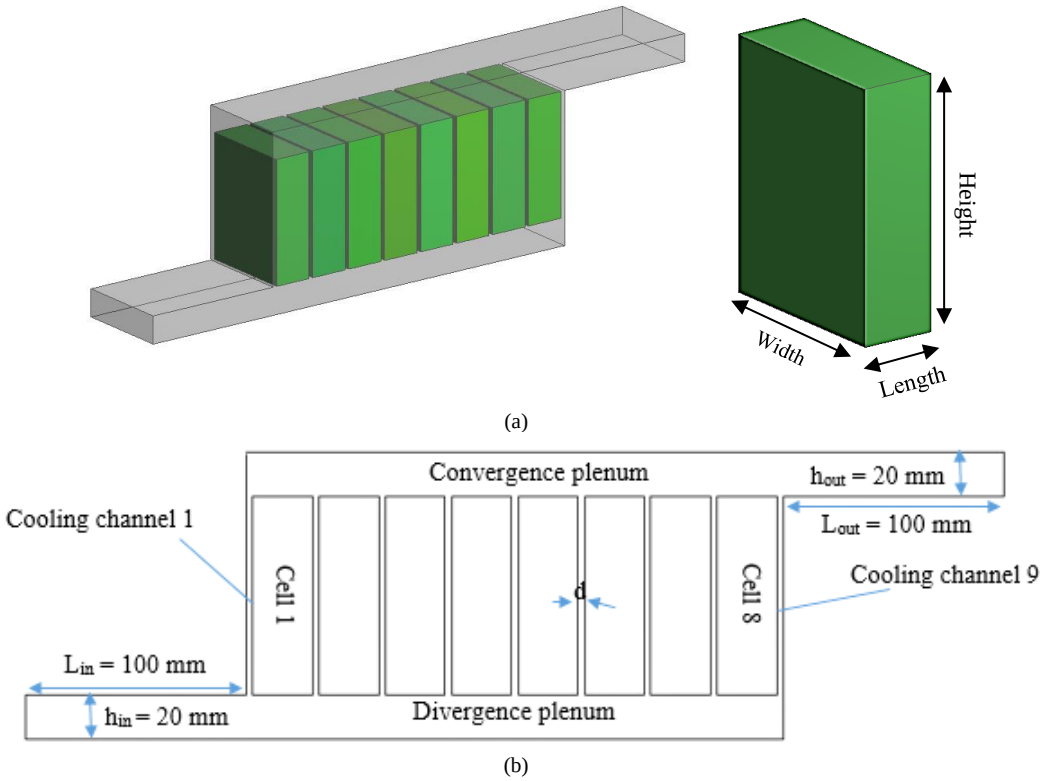

Figure 1. (a) A 3D standard Z-type BTMS and a cell, (b) 2D BTMS with schematic [13]

Table 1. Air and cell properties

Property	Air	Cell	Unit
Density	1.165	1542.9	kg/m^3
Specific heat	1005	1337	J/kgK
Dynamic viscosity	1.86×10^{-5}	-	kg/ms
Thermal conductivity	0.0267	21.1, 1.05	W/mK

According to the findings from the literature [13, 30, 33], air flow velocities in each cooling channel of the standard Z-type air-cooled BTMS are not uniform. The studies observed that the cooling channels closest to the outlet manifold absorb a significant amount of the airflow compared to those closest to the inlet manifold, which is not suitable for cooling homogeneity and could result in a significant difference in temperature between the cells. To influence the airflow distribution, Oyewola et al. [48] redesigned the divergence plenum into a step-like structure, covering the path that connects all of the cooling channels, thus altering the airflow path and creating an avenue for adequate flow of air to be sucked into the respective cooling channels, which in turn produces better cooling performance. The study focused on constant step heights of 2.5, 4, 5, and 10 mm derived from the height of the divergence plenum and the number of steps: 7 steps, 4 steps, 3 steps, and 1 step, respectively. The height of the step must be an integer to achieve steps of equal height. A detailed description of the design of the steps in the step-like BTMS can be obtained in the work of Oyewola et al. [48]. However, the study did not consider variable step height in all the cases. In the current study, variable step heights were considered for BTMS with 4 steps and 3 steps. Figure 2 displays the schematics of a 3-step BTMS model.

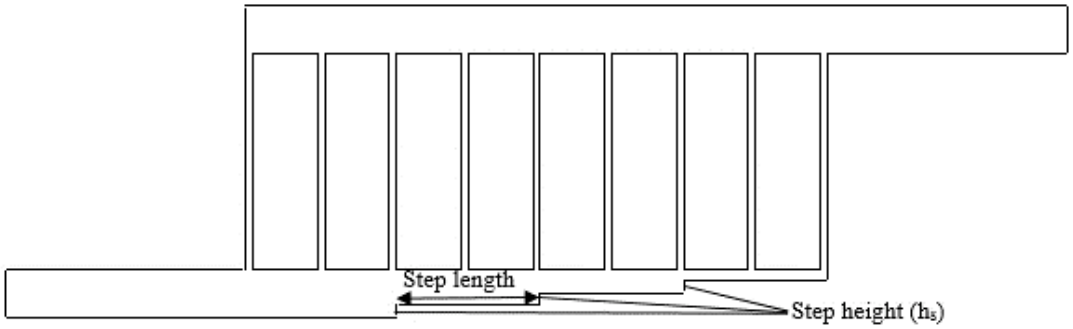

Figure 2. Step model [48]

2-2- Numerical Solution

2-2-1- Boundary Conditions and Assumptions

The velocity and temperature boundary conditions for the BTMS at the inlet were set to 3.5 m/s and 299.15 K, respectively, while the pressure-outlet boundary condition was assigned with atmospheric pressure as the surrounding pressure. An adiabatic and non-slip condition was assigned to the surrounding wall of the system, while a non-slip condition was assigned to the battery walls. The numerical solution also considered the following assumptions: (1) the physical properties of air and batteries are constant; (2) pressure and temperature remain constant in the surrounding environment; and (3) the batteries were considered to be a constant heat source, having a constant heat generation rate of 11.8 W.

2-2-2- Mesh Generation and Grid Sensitivity Study

A structural mesh with five inflation layers of first layer height (y^+) of 0.1mm at both the system and battery walls, to account for boundary layers, was generated. Based on the settings, a grid sensitivity analysis was carried out to assure a solution-independent grid. Figure 3 shows the selected grid of the standard BTMS. In order assess the sensitivity of the grid, the ΔT_{max} and T_{min} of the standard BTMS were employed. As the grid number increases above 118,016, as shown in Figure 4, ΔT_{max} and T_{max} become more stable with deviations less than 0.01 K and 0.02 K, respectively. Hence, a model with a 118,016 mesh size was chosen and used in this study.

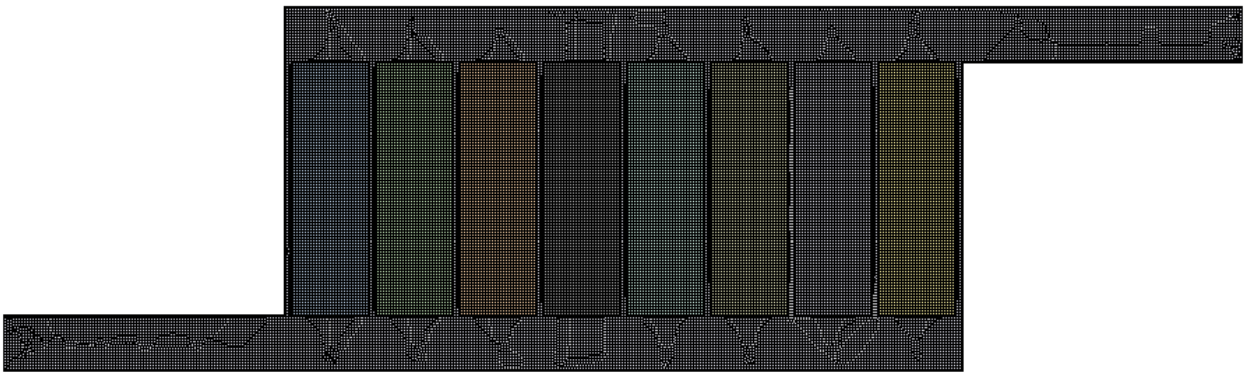

Figure 3. Selected grid

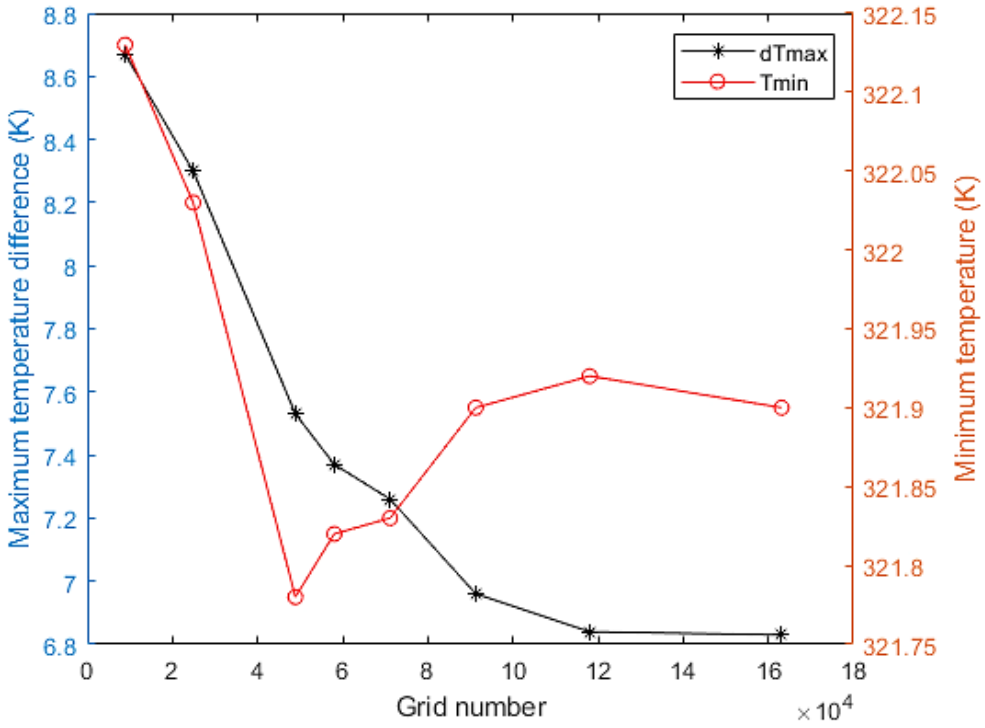

Figure 4. Grid sensitivity chart

2-2-3- Numerical Method

In order to simulate the model's flow and temperature profile, ANSYS Fluent, a CFD solver, was used. The T_{max} and $\Delta T_{max}$of the BTMS serve as the performance indexes for this investigation. The time-dependent flow problem was solved using the governing equations [49], such as continuity (Equation 1) and momentum Equations 2, while the thermal problem of the airflow was resolved using the energy conservation Equation 3:

$$\nabla.\vec{v} = 0 \tag{1}$$

$$\rho\frac{\overrightarrow{dv}}{dt} = -\nabla p + \mu\nabla^2\vec{v} \tag{2}$$

$$\rho c\frac{\partial T}{\partial t} + \nabla.(\rho c\vec{v}T) = \nabla.(\mathrm{k}\nabla\mathrm{T}) \tag{3}$$

where p, T, and $\vec{v}$ are the static pressure, temperature, and velocity of the cooling air; ρ, μ, k, and c are the air properties, which are density, dynamic viscosity, thermal conductivity, and specific heat, respectively. The Reynolds number (Equation 4) was estimated to be 6795 based on the inlet flow velocity of 3.5 m/s and the inlet manifold height. Hence the flow is considered to be turbulent, and an enhanced wall treatment [49] with the standard k-ε model (Equations 5 and 6) was chosen as the turbulence model.

$$Re = \frac{\rho v h_{in}}{\mu} \tag{4}$$

Turbulent kinetic energy equation:

$$\frac{\partial}{\partial t}(\rho k_t) + \frac{\partial}{\partial x_j}(\rho k_t u_j) = \frac{\partial}{\partial x_j}\left(\left(\mu + \frac{\mu_t}{\alpha_{k_t}}\right)\frac{\partial k_t}{\partial x_j}\right) + G_{k_t} + G_b - \rho\varepsilon - Y_M + S_{k_t} \tag{5}$$

Turbulent kinetic energy dissipation equation:

$$\frac{\partial}{\partial t}(\rho\varepsilon) + \frac{\partial}{\partial x_j}(\rho\varepsilon u_j) = \frac{\partial}{\partial x_j}\left(\left(\mu + \frac{\mu_t}{\alpha_\varepsilon}\right)\frac{\partial \varepsilon}{\partial x_j}\right) + C_{1\varepsilon}\frac{\varepsilon}{k_t}(G_{k_t} + C_{3\varepsilon} + G_b) - \rho C_{2\varepsilon}\frac{\varepsilon^2}{k_t} - S_\varepsilon \tag{6}$$

where $G_{k_t}\ and\ G_b$ are the turbulent kinetic energy generation caused by mean velocity and the turbulent kinetic energy generation as a result of buoyancy effects, respectively; u_j is the jth component of the velocity vector; μ and $\mu_t$are the molecular and turbulent dynamic viscosities; and k_t and ε are the turbulent kinetic energy and turbulence dissipation rate, respectively; S_{k_t} and S_ε are the source terms of k_t and ε, respectively; $\alpha_{k_t}$and α_ε are the inverse effective Prandtl numbers for k_t and ε, respectively; and $C_{1\varepsilon}, C_{2\varepsilon}, and\ C_{3\varepsilon}$ are empirical constants. Y_M represents the influence of the fluctuating dilation incompressible turbulent to the sum of dissipation rates.

For the battery cells, the energy conservation equation [27] (Equation 7) is:

$$\rho_b c_b\frac{\partial T}{\partial t} = \nabla.(k_b\nabla T) + Q \tag{7}$$

where Q, k_b, c_b, and ρ_b, represents heat generated, the battery's specific heat capacity, its thermal conductivity, and its density, respectively.

In addition, when solving the governing equations, the solver took into account the SIMPLE algorithm. The central-differencing and second-order terms, were employed to discretize the convective and diffusive terms. More so, the flow and energy terms convergence requirements were set at 10^{-5} and 10^{-8}, respectively. Figure 5 shows the flowchart of the solution methodology.

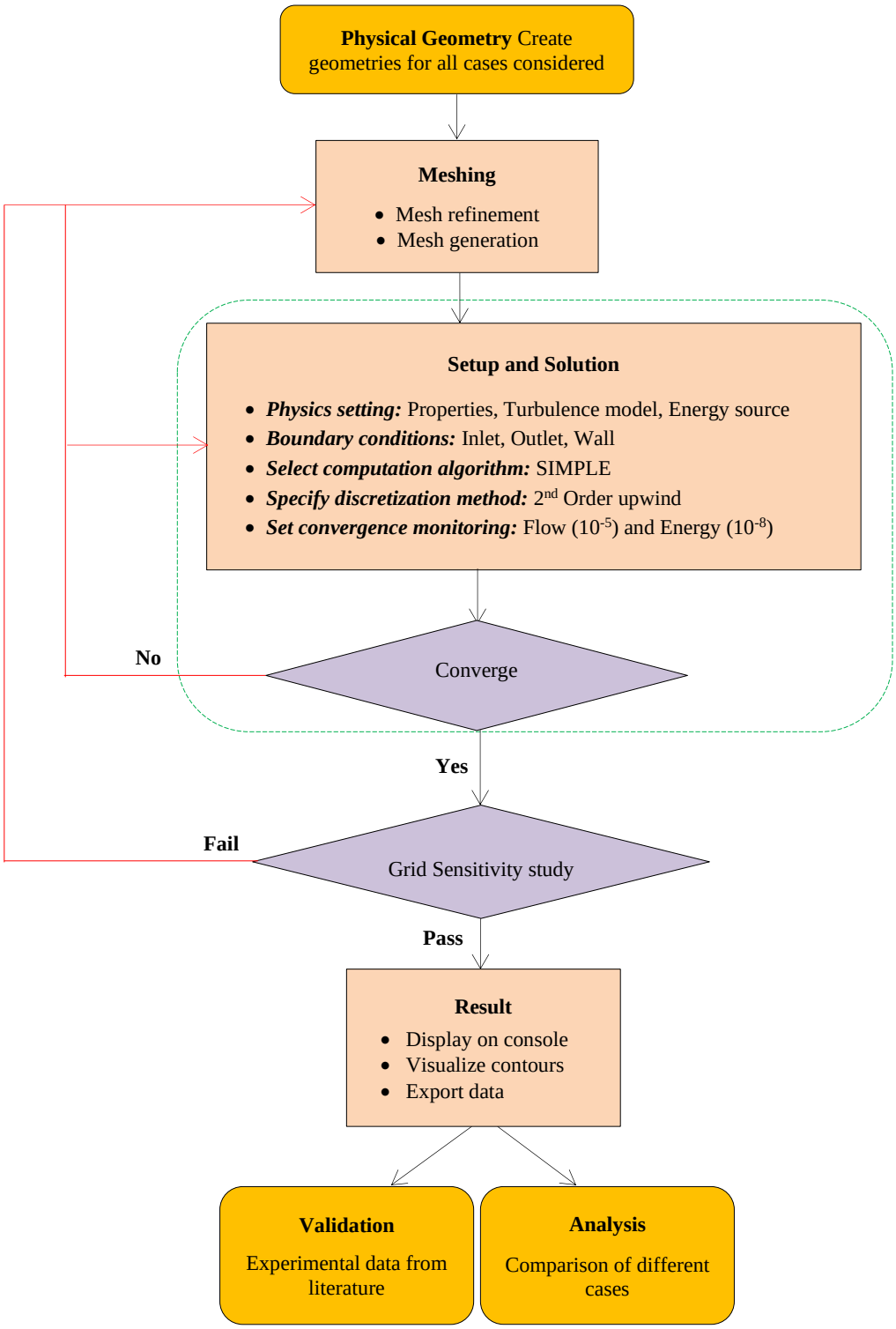

Figure 5. Methodology Flowchart

3- Results and Discussion

3-1- Validation of the Numerical Model

The experiment by Chen et al. [13] was carried out for the Z-type BTMS and the ΔT_{max} and ΔT_{min} were measured, from the second and eighth batteries of the battery pack, respectively. The experiments were further done for three inlet velocities of 3, 3.5, and 4 m/s. In the experiment, the batteries were represented by blocks, while K-type thermocouples were placed on the center of each block to measure temperatures. Simulations were conducted with parameters similar to those of the experiment, to test the validity of the numerical model. A comparison of the simulation results and experimental results are shown in Figure 6. The ΔT_{max} and ΔT_{min} were found to have average errors of 0.9 K and 0.6 K, respectively, which falls within an acceptable range, thus confirming the validity and acceptability of the numerical solution procedure employed.

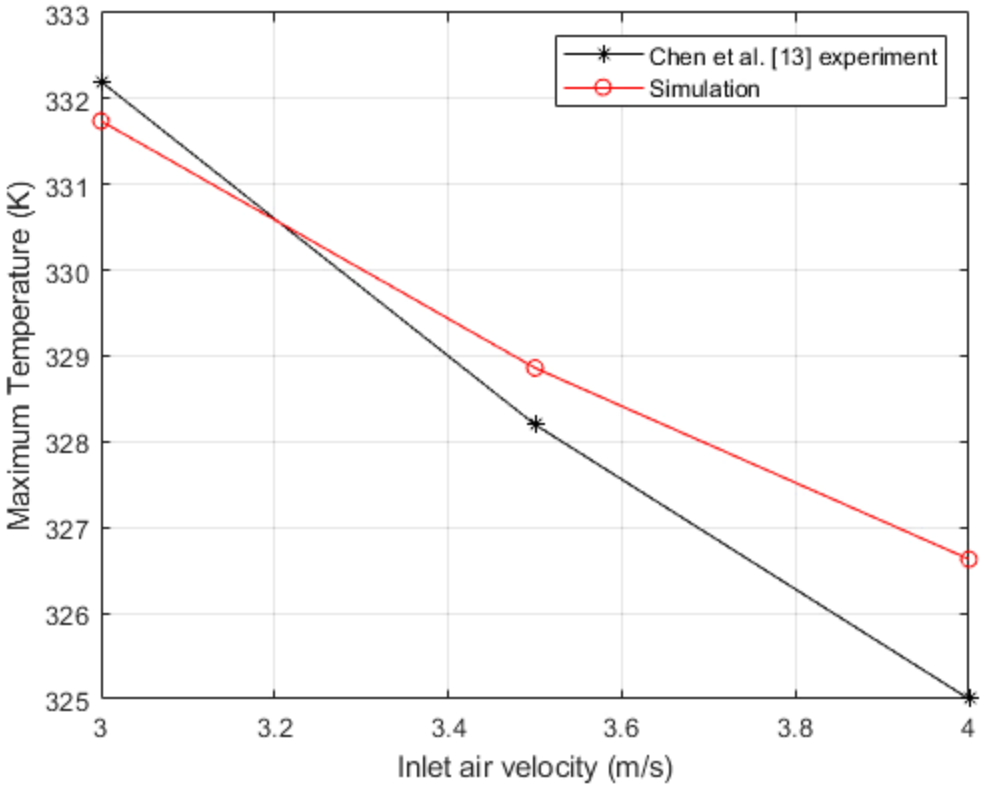

(a)

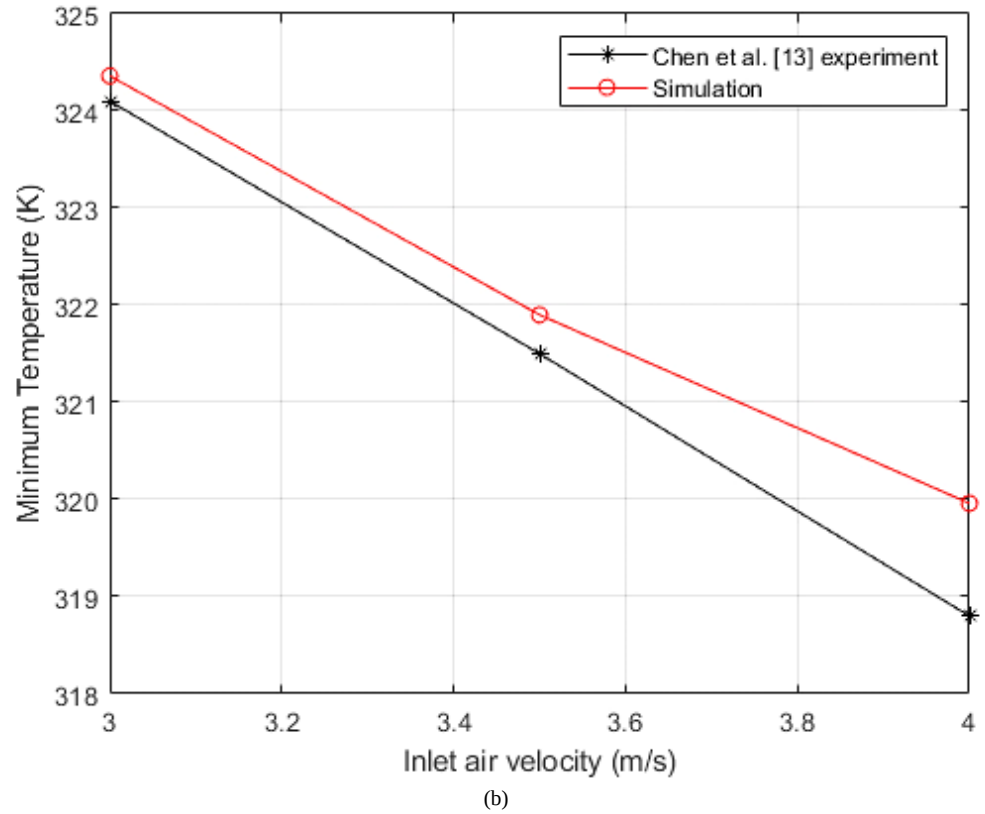

(b)

Figure 6. Experimental [13] and present simulation results comparison: (a) T_{max}, (b) T_{min}

The standard model's temperature and velocity contours are displayed in Figures 7-a and 7-b, respectively. The T_{max}, $\Delta T_{max,}$ and ΔP values are328.86 K, 6.96 K, and 22.15 Pa, respectively. It can be seen from Figure 7-a that the first four batteries in the battery pack have a very high temperature compared to the remaining batteries as a result of an uneven distribution of airflow into the cooling channels leading poor thermal homogeneity and decreasing the BTMS's ability to effectively cool the system.

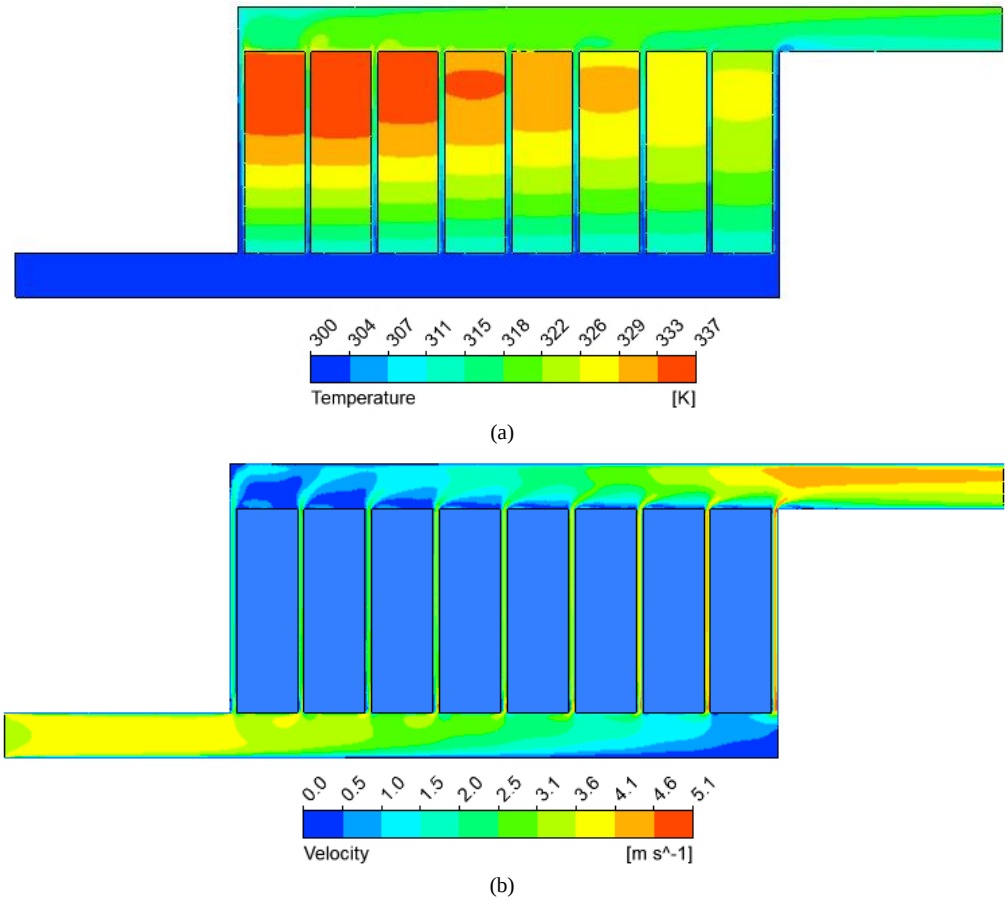

Figure 7. Contours of the standard model: (a) temperature; (b) velocity

3-2- Influence of Variable Step Height on The Temperature of the Batteries

Generally, the variable height configuration was adopted based on the sum of the step heights for the conventional BTMS models for the 3-step model, the total step height in the divergence plenum is 15 mm, while that of the 4-step model is 16 mm. The basic principle taken into consideration is the reduction in cross-sectional area of air passage due to the step design. To evaluate the impact of variable step height on the system, the pressure drop is being target for reduction, due to the resistance caused by the steps.

3-2-1- The 3-step BTMS Model

As stated earlier, three different step heights were selected and assigned to each height of the 3-steps model, while ensuring that the sum of the heights is 15 mm. The first, second and third heights are denoted as H1, H2 and H3, respectively as shown in Table 2.

Table 2. Variable height arrangement for the 3-step BTMS model

Cases	H1 (mm)	H2 (mm)	H3 (mm)
0	5	5	5
1	3	6	6
2	4	5	6
3	5	4	6
4	5	6	4
5	6	3	6
6	6	5	4
7	3	5	7
8	5	7	3
9	7	3	5
10	3	7	5
11	5	3	7
12	7	5	3
13	4	6	5

Case 0 is the initial configuration of constant step height for the 3-step model having T_{max}, ΔT_{max}, and ΔP values of 325.28 K, 1.15 K, and 26.63 Pa, respectively. The temperature contour of case 0 is presented in Figure 8. By observing the temperature contour for standard BTMS (Figure 7-a) and the case 0 BTMS (Figure 8), it can be clearly seen that the latter represent uniform temperature distribution on the battery cells, which indicates thermal homogeneity. Case 1 to Case 13 represent the various step height configurations for this model. As shown in Table 3, cases 1, 2, 10, and 13 show better cooling performance and lower power consumption in terms of thermal homogeneity and pressure drop, respectively, when compared to case 0. These four cases show an improvement from the performance of case 0, with case 1 having $\Delta T_{max}$and ΔP values of 0.9 K and 25.72 Pa, respectively. When considering T_{max}, the reduction, it was insignificant. Also, when compared to the standard Z-type model, Case 1 performed far better with a reduction of 3.58 K and 87.1% in terms of T_{max} and $\Delta T_{max,}$ respectively.

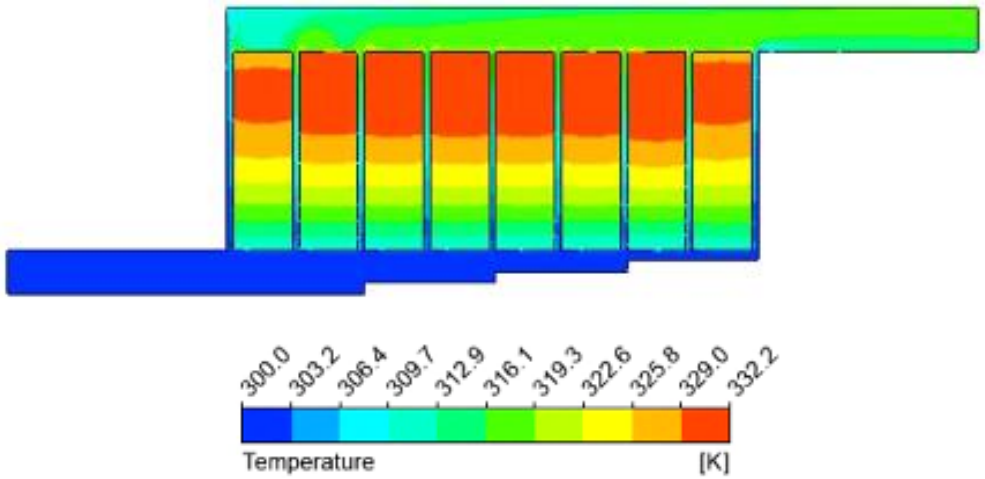

Figure 8. Temperature contour of a 3-step BTMS model

Table 3. Performance evaluation of various step height settings for a 3-step BTMS model

Cases	T_{max} (K)	ΔT_{max} (K)	ΔP(Pa)
0	325.28	1.15	26.63
1	325.44	0.90	25.72
2	325.40	0.94	25.96
3	325.46	1.09	26.31
4	325.60	1.77	27.22
5	325.74	1.64	26.74
6	325.60	1.96	27.66
7	325.69	1.31	25.45
8	326.57	3.12	27.83
9	325.86	2.40	27.64
10	325.46	0.92	26.08
11	325.73	1.45	26.09
12	326.44	3.56	28.68
13	325.32	0.91	26.36

As shown in Figure 9, airflow distribution in each cooling channel is influenced by the height of the steps, especially that of the first and second steps, which cover cooling channels 3 to 7. The first two cooling channels, denoted as index 1 and 2, respectively in Figure 9-a, and the last two cooling channels, denoted as index 8 and 9, respectively, of the four cases behaved in a similar pattern. The second step is higher than the first step in all four configurations, and varying the height of the steps with the consideration of H2 > H1 and with H1 not set relatively high can boost the airflow in the cooling channel at the mid-section of the BTMS.

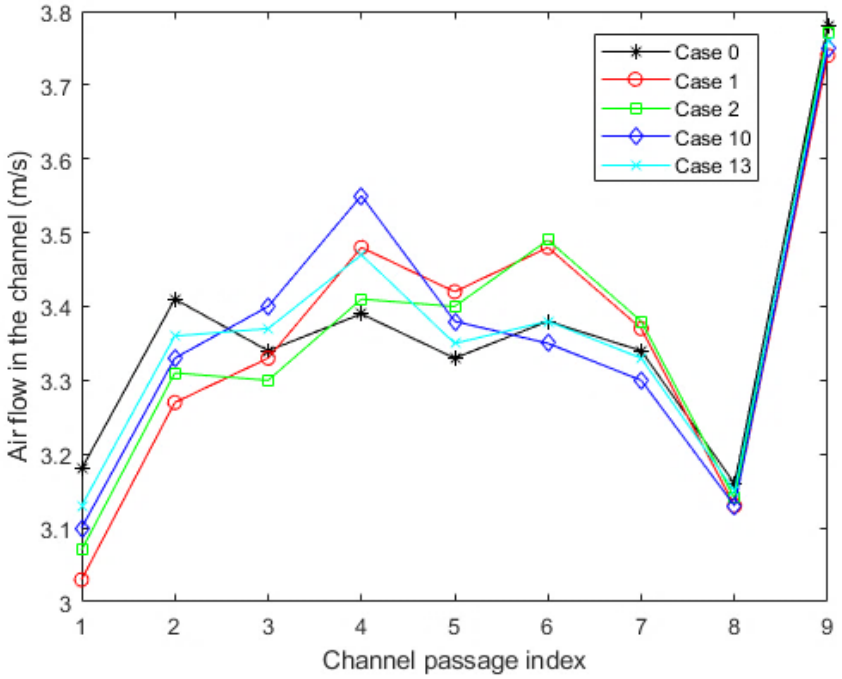

(a)

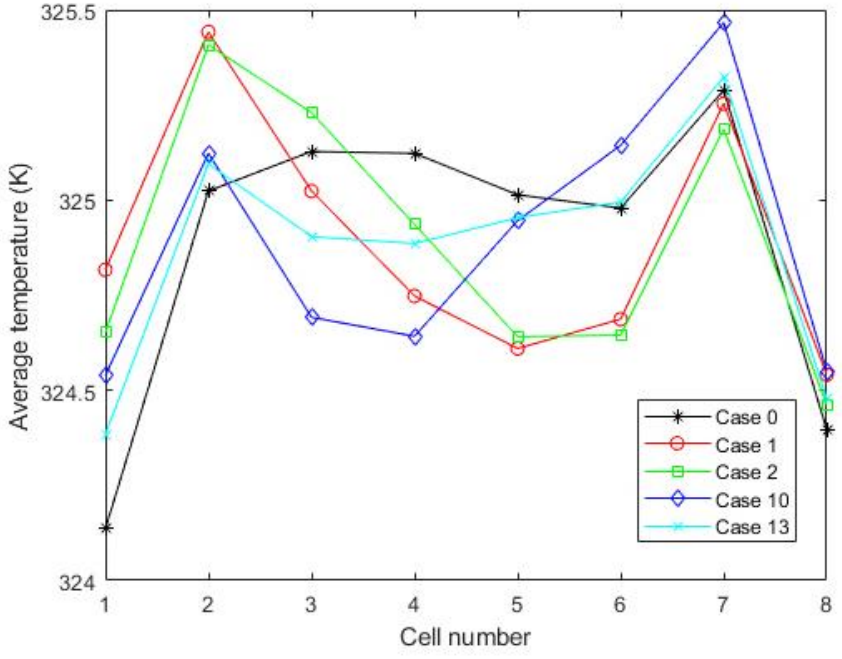

(b)

Figure 9. (a) Airflow and (b) temperature variation of 3-step BTMSs models

The general performance of the 3-step model as presented in Table 3, revealed series of variation in the predicted values of T_{max}, $\Delta T_{max}$and ΔP. Basically, redesign of the divergence plenum is done to minimize the T_{max} while the battery is in operation. This has been achieved by many researchers, and often accompanied by reduction of ΔT_{max}, signify thermal homogeneity among the batteries in the battery pack. In the same vein, reduction in the ΔT_{max} also comes with increase in ΔP. However, a design with the minimum T_{max} may not produce the best thermal homogeneity, when compared with another design. For instance, in table 3, BTMS with equal height of step, i.e. case 0, produced the minimum value of $T_{max} = 325.28\,K$, while $\Delta T_{max} = 1.15\,K$ and $\Delta P = 26.63\,Pa$. Considering pumping power consumption, case 0 is not considered economical when compared with case 1 with $\Delta P = 25.72\,Pa$. For case 1, the T_{max} is 325.44 K, which represent a difference of 0.12 K when compared to case 0. The temperature difference between T_{max} of case 0 and case 1 is insignificant, however the difference in ΔP cannot be overlooked as cost of pumping will certainly vary. Cases such as cases 2, 3 and 10 produced lower values of ΔT_{max} than the initial case 0 with equal height of steps. Similarly, cases 2, 7, 10, 11 and 13 produced lower values of ΔP when compared to case 0. These findings will be of great significance on systems were improvement in thermal homogeneity and reduction in pumping cost are of primary concern.

3-2-2- The 4-step BTMS Model

For the 4-step models, the sum of the step heights for each model is 16 mm Table 4 listed the variable height configurations for the models.

Table 4. Variable height arrangement for the 4-step BTMS model

Cases	H1 (mm)	H2 (mm)	H3 (mm)	H4 (mm)
14	4	4	4	4
15	3	3	5	5
16	3	4	4	5
17	3	4	5	4
18	3	5	3	5
19	4	4	5	3
20	4	3	5	4
21	4	4	3	5
22	5	3	5	3
23	5	4	3	4
24	5	3	3	5
25	3	5	5	3
26	3	5	4	4
27	4	5	4	3
28	4	3	4	5
29	4	5	3	4
30	5	5	3	3
31	5	4	4	3
32	5	3	4	4

Cases 15 to 32 show the various step height configurations, while case 14 represents the initial 4-step model with constant step height, with T_{max}, ΔT_{max}, and ΔP values of 325.19 K, 0.95 K, and 26.48 Pa, respectively. Figure 10 shows the temperature contour of case 14. Similarly, by observing the temperature contour for standard BTMS (Figure 7-i) and case 14 BTMS (Figure 10), it can be clearly seen case 14 produced a better thermal homogeneity. The variables H1, H2, H3 and H4 represents the heights of the first, second, third and fourth steps, respectively. As shown in Table 5, none of the cases shows improved performance when compared to the default height configuration (case 14). Regarding thermal homogeneity, no case outperformed case 14, though, some cases performed slightly better in the area of T_{max} and power consumption, however, their improvements are relatively insignificant.

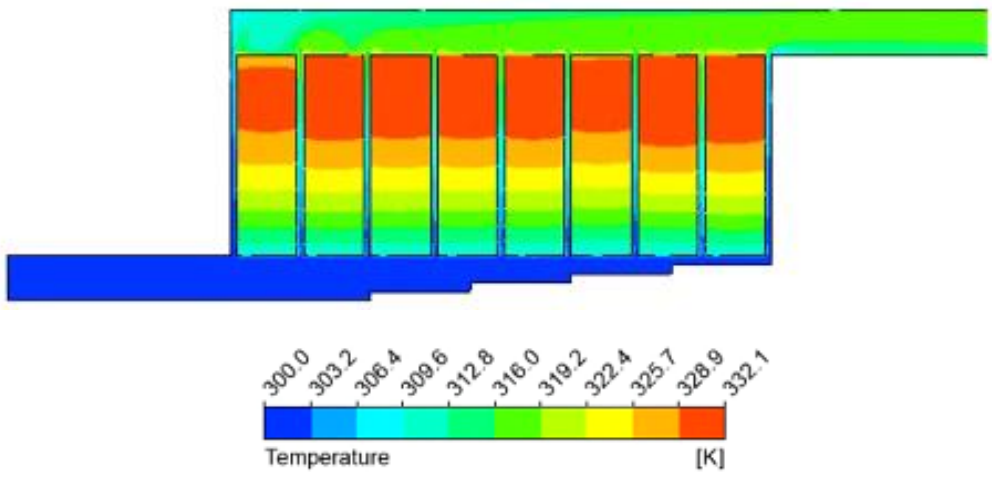

Figure 10. Temperature contour of a 4-step BTMS model

Table 5. Performance evaluation of various step height settings for a 4-step BTMS model

Cases	T_{max} (K)	ΔT_{max}(K)	ΔP (Pa)
14	325.19	0.95	26.48
15	325.68	1.89	25.60
16	325.47	1.59	25.75
17	325.30	1.12	26.00
18	325.23	1.22	25.94
19	325.88	1.81	26.79
20	325.30	1.10	26.24
21	325.18	1.19	26.13
22	325.83	1.91	27.06
23	325.24	1.29	26.95
24	325.32	1.40	26.42
25	325.90	1.65	26.58
26	325.32	0.99	26.18
27	325.87	1.93	27.05
28	325.43	1.57	25.95
29	325.30	1.18	26.71
30	325.73	2.25	27.69
31	325.78	2.05	27.29
32	325.18	1.02	26.68

It is worth noting that case 26 (3-5-4-4) having T_{max}, ΔT_{max}, and ΔP values of 325.32 K, 0.99 K, and 26.18 Pa, respectively performed relatively similar to case 14 with little improvement in power consumption only. However, when compared to the standard BTMS model, case 26 outperformed with an improvement of 3.54 K and 85.8% in terms of T_{max} and ΔT_{max}, respectively. This performance shows improvement in design when compared to the work of Zhang et al. [20], where T_{max} and ΔT_{max} were reduced by 1.84 and 3.66 K, respectively. Although as seen from the table, case 21 performed better than all the cases when considering T_{max}, however it does not give the best performance in terms of ΔT_{max} and ΔP. Figures 11-a and 11-b display the similarity observed in the performances of case 14 and case 26.

3-3- Effect of Inlet Velocity on the Performance of Selected Cases

For some selected cases, such as cases 0, 1, 14, and 26, T_{max} of the cases decreases as the flow velocity increases. Though Case 0 offers the lowest T_{max} for all velocities, Case 26 significantly improved in T_{max}, at a higher velocity surpassing case 14 at velocities above 3.7 m/s as seen in Figure 12-a. For all selected cases and across all velocities, a reduction is seen for the maximum temperature difference. Case 0 provided the highest ΔT_{max} across all studied velocities, however, when compared to case 1 at higher velocities (> 4.8 m/s), case 0 performs better. It is worth noting that the reduction observed in the ΔT_{max} for case 1 occurs at a slow pace across the studied velocities. Considering the behavior of cases 14 and 26, it was observed that case 14 performed better except at velocities above 4.6 m/s, where case 26 outperformed it. As shown in Figure 12, case 26 improved greatly at higher velocities above 4.6 m/s than the other cases. Generally, for cases with variable step height settings, case 26 provides better performance and improvement in terms of T_{max} than case 1 across all velocities, and also, for the ΔT_{max}, case 1 outperformed case 26 at lower velocities but performed woefully at velocities above 4.4 m/s. From figure 12-b, it can be observed that case 26 will provide the best thermal uniformity at higher velocities than the other cases.

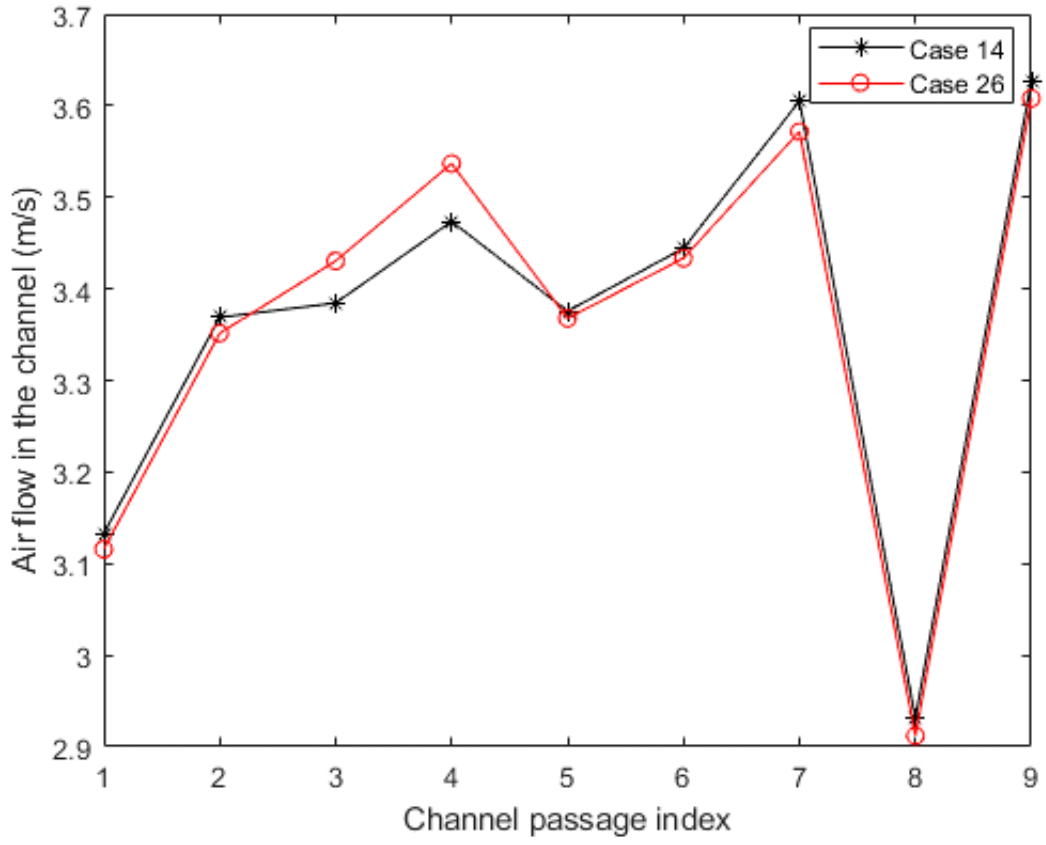

(a)

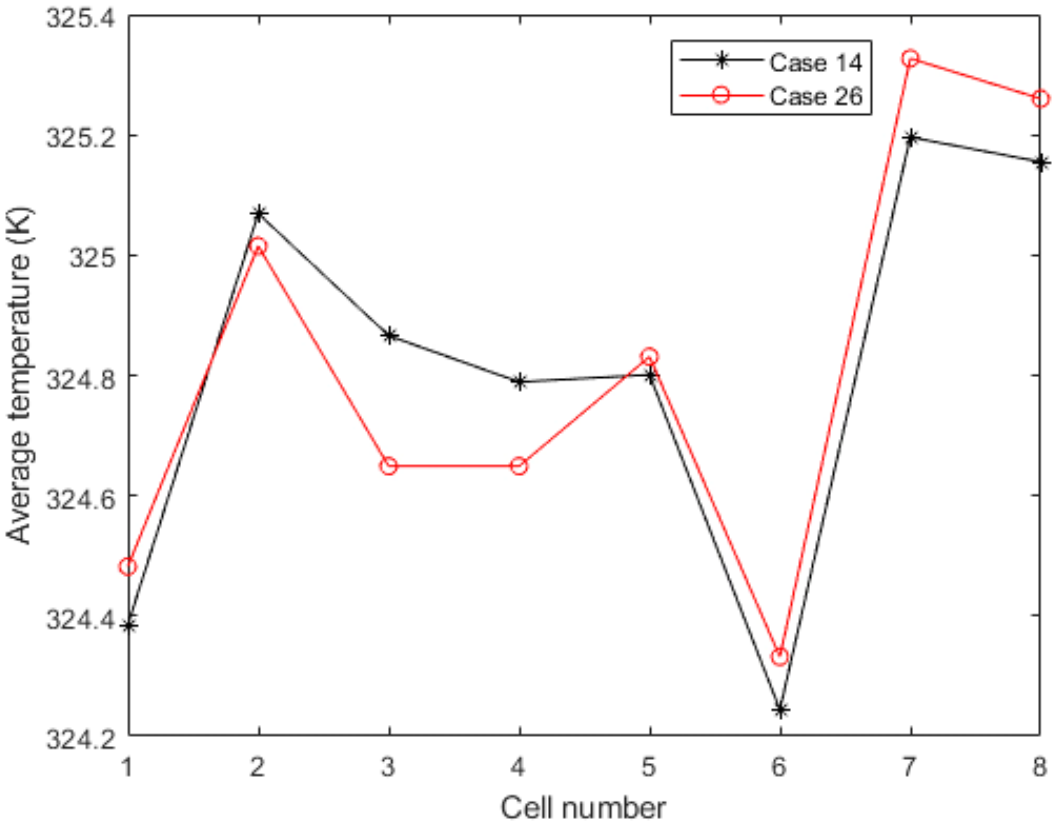

(b)

Figure 11. Airflow and temperature variation of cases 14 and 26 of the 4-step BTMS model

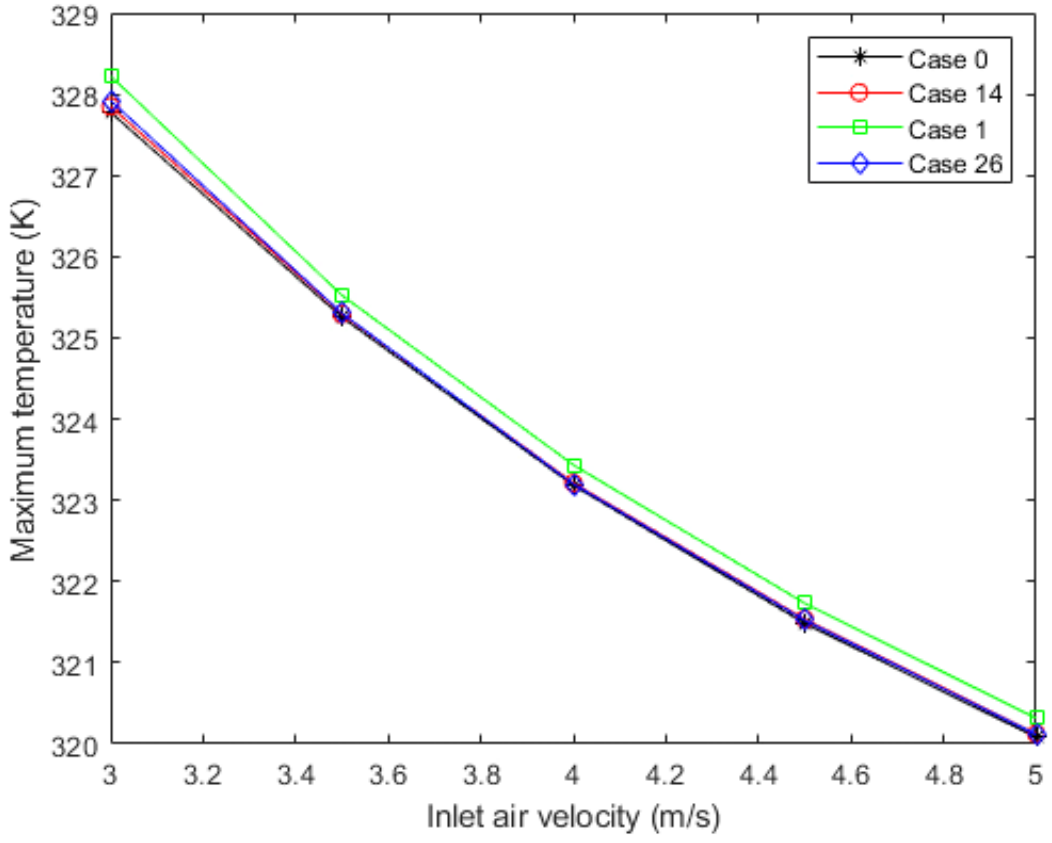

(a)

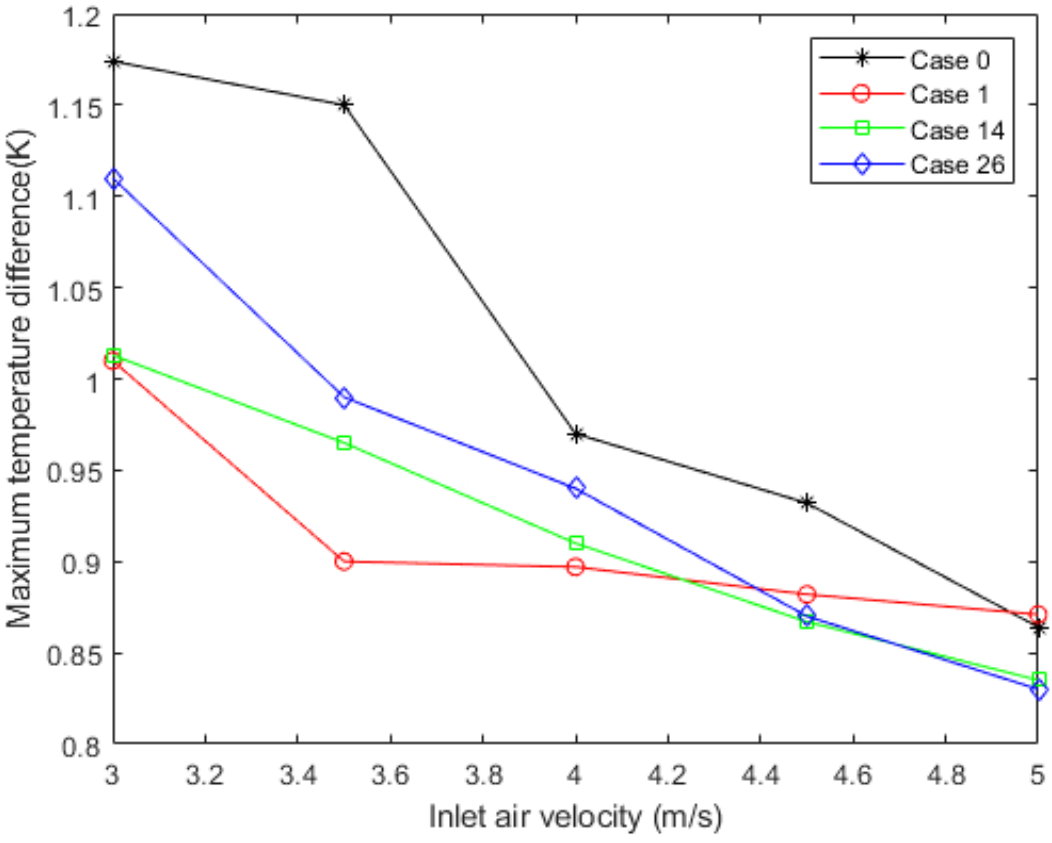

(b)

Figure 12. (a) T_{max} and (b) ΔT_{max} comparison for several cases with various inlet flow velocities

4- Conclusions

In this study, the scope of research on the existing step-like divergence plenum design of Z-type BTMS [48], with equal height of steps, was extended by varying the height of steps. Studies were carried out to minimize the ΔP while still achieving reasonable cooling efficiency in terms of reducing the maximum temperature of the battery in the battery pack. The CFD methodology was adopted, which was validated by comparing estimated $\Delta T_{max}$and $T_{max}$with experimental data from the literature. Two types of step-like models; 3-step and 4-step, each with varying step heights, were considered. Furthermore, under higher inlet air velocities, the performance of each case was examined. The following findings were made from this study:

- For a three steps BTMS (3-step model), design with step heights 3, 6, and 6 mm (case 1) offered the minimum ΔP and ΔT_{max}, and when compared with the model with constant step height of 5 mm (case 0), yielded reduction by 3.4% and 21.6%, respectively.
- The designs with four steps did not show any significant improvement. However, the configuration with step heights 3, 5, 4, and 4 mm (case 26) showed a relatively similar trait to that of the default model with constant step height of 4 mm (case 14).
- By increasing the inlet airflow velocity, the cooling efficiency of the four steps BTMS cases was improved. The T_{max} and ΔT_{max}values of all the systems showed a downward trend, however, ΔT_{max} for case 1 began to perform poorly at greater inlet flow velocities. The best cooling improvement was seen in case 26 at velocities over 3.7 m/s for T_{max} and velocities over 4.8 m/s for ΔT_{max}.

5- Nomenclature

Acronym		
HCS	Hybrid Cooling Strategy	
MCPs	Mini-channel cold plates	
UAV	Unmanned Aerial Vehicles	
CFD	Computational Fluid Dynamics	
EV	Electric Vehicles	
PCM	Phase Change Material	
2D	Two Dimensional	
3D	Three Dimensional	
BTMS	Battery Thermal Management System	
Symbols		
H1	Height of firs step	mm
H2	Height of second step	mm
H3	Height of third step	mm
H4	Height of fourth step	mm
H	Height	mm
D	Width of cooling channel	mm
L	Length	mm
$\boldsymbol{P}$	Average pressure	Pa
$\boldsymbol{v}$	Air velocity at inlet	m/s
$\boldsymbol{u}$	Velocity vector	m/s
$\boldsymbol{x}$	x-coordinate	m
Re	Reynolds number	-
$\boldsymbol{T}$	Temperature	K
$\boldsymbol{t}$	Time	s
$\boldsymbol{Q}$	Rate of heat generation	W
$\boldsymbol{k}$	Thermal conductivity	W/mK
C	Specific heat capacity	J/kgK
$\boldsymbol{G_k}$ and $\boldsymbol{G_b}$	Turbulence kinetic energy generation due to the average velocity gradients and buoyancy effects respectively	
$\boldsymbol{Y_M}$	Contribution of fluctuating dilatation in compressible turbulence to overall dissipation rate	
$\boldsymbol{C_{1\varepsilon}, C_{2\varepsilon}, C_{3\varepsilon}}$	Model constants	
$\boldsymbol{S_k}$ and $\boldsymbol{S_\epsilon}$	Source terms	

Greek letters		
$\boldsymbol{\rho}$	Density	kg/m^3
$\boldsymbol{\mu}$	Dynamic viscosity	kg/ms
$\boldsymbol{\sigma_k}$, $\boldsymbol{\sigma_\epsilon}$	k and ε turbulent Prandtl numbers	
Δ	Change/Difference	
$\boldsymbol{\nabla}$	Gradient operator	
Subscripts		
B	Battery	
$\boldsymbol{s}$	Step	
In	Inlet of plenum	
out	Outlet or plenum	
$\boldsymbol{max}$	Maximum	
$\boldsymbol{min}$	Minimum	

6- Declarations

6-1- Author Contributions

Conceptualization, O.O.; methodology, O.O., A.A., and A.I.; software, O.O., A.A., and A.I.; validation, O.O., A.A., and A.I.; formal analysis, O.O., A.A., and A.I.; investigation, O.O., A.A., and A.I.; resources, O.O.; data curation, O.O., A.A., and A.I.; writing—original draft preparation, O.O., A.A., and A.I.; writing—review and editing, O.O., A.A., and A.I.; visualization, O.O.; supervision, O.O.; project administration, O.O.; funding acquisition, O.O. All authors have read and agreed to the published version of the manuscript.

6-2- Data Availability Statement

The data presented in this study are available on request from the corresponding author.

6-3- Funding

The authors received no financial support for the research, authorship, and/or publication of this article.

6-4- Institutional Review Board Statement

Not applicable.

6-5- Informed Consent Statement

Not applicable.

6-6- Conflicts of Interest

The authors declare that there is no conflict of interest regarding the publication of this manuscript. In addition, the ethical issues, including plagiarism, informed consent, misconduct, data fabrication and/or falsification, double publication and/or submission, and redundancies have been completely observed by the authors.

7- References

[1] Na, X., Kang, H., Wang, T., & Wang, Y. (2018). Reverse layered air flow for Li-ion battery thermal management. Applied Thermal Engineering, 143, 257–262. doi:10.1016/j.applthermaleng.2018.07.080.

[2] Dan, D., Yao, C., Zhang, Y., Zhang, H., Zeng, Z., & Xu, X. (2019). Dynamic thermal behavior of micro heat pipe array-air cooling battery thermal management system based on thermal network model. Applied Thermal Engineering, 162, 114183. doi:10.1016/j.applthermaleng.2019.114183.

[3] Zhong, G., Zhang, G., Yang, X., Li, X., Wang, Z., Yang, C., Yang, C., & Gao, G. (2017). Researches of composite phase change material cooling/resistance wire preheating coupling system of a designed 18650-type battery module. Applied Thermal Engineering, 127, 176–183. doi:10.1016/j.applthermaleng.2017.08.022.

[4] Wang, Y., Dan, D., Zhang, Y., Qian, Y., Panchal, S., Fowler, M., Li, W., Tran, M. K., & Xie, Y. (2022). A novel heat dissipation structure based on flat heat pipe for battery thermal management system. International Journal of Energy Research, 46(11), 15961–15980. doi:10.1002/er.8294.

[5] Boonma, K., Patimaporntap, N., Mbulu, H., Trinuruk, P., Ruangjirakit, K., Laoonual, Y., & Wongwises, S. (2022). A Review of the Parameters Affecting a Heat Pipe Thermal Management System for Lithium-Ion Batteries. Energies, 15(22), 8534. doi:10.3390/en15228534.

[6] Wang, C., Zhang, G., Meng, L., Li, X., Situ, W., Lv, Y., & Rao, M. (2017). Liquid cooling based on thermal silica plate for battery thermal management system. International Journal of Energy Research, 41(15), 2468–2479. doi:10.1002/er.3801.

[7] Panchal, S., Khasow, R., Dincer, I., Agelin-Chaab, M., Fraser, R., & Fowler, M. (2017). Thermal design and simulation of mini-channel cold plate for water cooled large sized prismatic lithium-ion battery. Applied Thermal Engineering, 122, 80–90. doi:10.1016/j.applthermaleng.2017.05.010.

[8] Rao, Z., Qian, Z., Kuang, Y., & Li, Y. (2017). Thermal performance of liquid cooling based thermal management system for cylindrical lithium-ion battery module with variable contact surface. Applied Thermal Engineering, 123, 1514–1522. doi:10.1016/j.applthermaleng.2017.06.059.

[9] Jilte, R. D., Kumar, R., Ahmadi, M. H., & Chen, L. (2019). Battery thermal management system employing phase change material with cell-to-cell air cooling. Applied Thermal Engineering, 161, 114199. doi:10.1016/j.applthermaleng.2019.114199.

[10] Bais, A. R., Subhedhar, D. G., Joshi, N. C., & Panchal, S. (2022). Numerical investigation on thermal management system for lithium ion battery using phase change material. Materials Today: Proceedings, 66(4), 1726–1733. doi:10.1016/j.matpr.2022.05.269.

[11] Akinlabi, A. A. H., & Solyali, D. (2020). Configuration, design, and optimization of air-cooled battery thermal management system for electric vehicles: A review. Renewable and Sustainable Energy Reviews, 125, 109815. doi:10.1016/j.rser.2020.109815.

[12] Erb, D. C., Kumar, S., Carlson, E., Ehrenberg, I. M., & Sarma, S. E. (2017). Analytical methods for determining the effects of lithium-ion cell size in aligned air-cooled battery packs. Journal of Energy Storage, 10, 39–47. doi:10.1016/j.est.2016.12.003.

[13] Chen, K., Wu, W., Yuan, F., Chen, L., & Wang, S. (2019). Cooling efficiency improvement of air-cooled battery thermal management system through designing the flow pattern. Energy, 167, 781–790. doi:10.1016/j.energy.2018.11.011.

[14] Behi, H., Karimi, D., Behi, M., Ghanbarpour, M., Jaguemont, J., Sokkeh, M. A., Gandoman, F. H., Berecibar, M., & Van Mierlo, J. (2020). A new concept of thermal management system in Li-ion battery using air cooling and heat pipe for electric vehicles. Applied Thermal Engineering, 174, 115280. doi:10.1016/j.applthermaleng.2020.115280.

[15] Li, X., He, F., Zhang, G., Huang, Q., & Zhou, D. (2019). Experiment and simulation for pouch battery with silica cooling plates and copper mesh based air cooling thermal management system. Applied Thermal Engineering, 146, 866–880. doi:10.1016/j.applthermaleng.2018.10.061.

[16] Jiaqiang, E., Yue, M., Chen, J., Zhu, H., Deng, Y., Zhu, Y., Zhang, F., Wen, M., Zhang, B., & Kang, S. (2018). Effects of the different air cooling strategies on cooling performance of a lithium-ion battery module with baffle. Applied Thermal Engineering, 144, 231–241. doi:10.1016/j.applthermaleng.2018.08.064.

[17] Wang, M., Teng, S., Xi, H., & Li, Y. (2021). Cooling performance optimization of air-cooled battery thermal management system. Applied Thermal Engineering, 195, 117242. doi:10.1016/j.applthermaleng.2021.117242.

[18] Hong, S., Zhang, X., Chen, K., & Wang, S. (2018). Design of flow configuration for parallel air-cooled battery thermal management system with secondary vent. International Journal of Heat and Mass Transfer, 116, 1204–1212. doi:10.1016/j.ijheatmasstransfer.2017.09.092.

[19] Shahid, S., & Agelin-Chaab, M. (2018). Development and analysis of a technique to improve air-cooling and temperature uniformity in a battery pack for cylindrical batteries. Thermal Science and Engineering Progress, 5, 351–363. doi:10.1016/j.tsep.2018.01.003.

[20] Zhang, F., Liu, P., He, Y., & Li, S. (2022). Cooling performance optimization of air-cooling lithium-ion battery thermal management system based on multiple secondary outlets and baffle. Journal of Energy Storage, 52(A). doi:10.1016/j.est.2022.104678.

[21] Wang, T., Tseng, K. J., & Zhao, J. (2015). Development of efficient air-cooling strategies for lithium-ion battery module based on empirical heat source model. Applied Thermal Engineering, 90, 521–529. doi:10.1016/j.applthermaleng.2015.07.033.

[22] Chen, K., Wang, S., Song, M., & Chen, L. (2017). Configuration optimization of battery pack in parallel air-cooled battery thermal management system using an optimization strategy. Applied Thermal Engineering, 123, 177–186. doi:10.1016/j.applthermaleng.2017.05.060.

[23] Li, M., Liu, Y., Wang, X., & Zhang, J. (2019). Modeling and optimization of an enhanced battery thermal management system in electric vehicles. Frontiers of Mechanical Engineering, 14(1), 65–75. doi:10.1007/s11465-018-0520-z.

[24] Chen, K., Chen, Y., She, Y., Song, M., Wang, S., & Chen, L. (2020). Construction of effective symmetrical air-cooled system for battery thermal management. Applied Thermal Engineering, 166, 114679. doi:10.1016/j.applthermaleng.2019.114679.

[25] Fan, Y., Bao, Y., Ling, C., Chu, Y., Tan, X., & Yang, S. (2019). Experimental study on the thermal management performance of air cooling for high energy density cylindrical lithium-ion batteries. Applied Thermal Engineering, 155, 96–109. doi:10.1016/j.applthermaleng.2019.03.157.

[26] Peng, X., Cui, X., Liao, X., & Garg, A. (2020). A thermal investigation and optimization of an air-cooled lithium-ion battery pack. Energies, 13(11), 2956. doi:10.3390/en13112956.

[27] Chen, K., Li, Z., Chen, Y., Long, S., Hou, J., Song, M., & Wang, S. (2017). Design of parallel air-cooled battery thermal management system through numerical study. Energies, 10(10), 1677. doi:10.3390/en10101677.

[28] Oyewola, O. M., Ismail, O. S., & Awonusi, A. A. (2022). Examination of Channel Angles Influence on the Cooling Performance of Air-cooled Thermal Management System of Li-Ion Battery. International Review of Mechanical Engineering, 16(4), 172–179. doi:10.15866/ireme.v16i4.22239.

[29] Xie, J., Ge, Z., Zang, M., & Wang, S. (2017). Structural optimization of lithium-ion battery pack with forced air-cooling system. Applied Thermal Engineering, 126, 583–593. doi:10.1016/j.applthermaleng.2017.07.143.

[30] Kharmale, S. B., Sathe, P. S., & Kolekar, Y. A. (2023). Effect of Cooling Conditions, Retrofitting on Strength of Concrete Subjected to Elevated Temperature. Civil Engineering Journal, 9(7), 1737-1752. doi:10.28991/CEJ-2023-09-07-013.

[31] Wang, M., Hung, T. C., & Xi, H. (2021). Numerical study on performance enhancement of the air-cooled battery thermal management system by adding parallel plates. Energies, 14(11), 3096. doi:10.3390/en14113096.

[32] Mba, E. J., Okeke, F. O., Ezema, E. C., Oforji, P. I., & Ozigbo, C. A. (2023). Post occupancy evaluation of ventilation coefficient desired for thermal comfort in educational facilities. Journal of Human, Earth, and Future, 4(1), 88-102. doi:10.28991/HEF-2023-04-01-07.

[33] Oyewola, O. M., Awonusi, A. A., & Ismail, O. S. (2022). Performance Improvement of Air-cooled Battery Thermal Management System using Sink of Different Pin-Fin Shapes. Emerging Science Journal, 6(4), 851–865. doi:10.28991/ESJ-2022-06-04-013.

[34] Mohammadian, S. K., & Zhang, Y. (2015). Thermal management optimization of an air-cooled Li-ion battery module using pin-fin heat sinks for hybrid electric vehicles. Journal of Power Sources, 273, 431–439. doi:10.1016/j.jpowsour.2014.09.110.

[35] Wang, N., Li, C., Li, W., Huang, M., & Qi, D. (2021). Effect analysis on performance enhancement of a novel air-cooling battery thermal management system with spoilers. Applied Thermal Engineering, 192, 116932. doi:10.1016/j.applthermaleng.2021.116932.

[36] Zhang, F., Lin, A., Wang, P., & Liu, P. (2021). Optimization design of a parallel air-cooled battery thermal management system with spoilers. Applied Thermal Engineering, 182, 116062. doi:10.1016/j.applthermaleng.2020.116062.

[37] Mousavi, S., Siavashi, M., & Zadehkabir, A. (2021). A new design for hybrid cooling of Li-ion battery pack utilizing PCM and mini channel cold plates. Applied Thermal Engineering, 197, 117398. doi:10.1016/j.applthermaleng.2021.117398.

[38] Yang, H., Li, M., Wang, Z., & Ma, B. (2023). A compact and lightweight hybrid liquid cooling system coupling with Z-type cold plates and PCM composite for battery thermal management. Energy, 263, 10 1016. doi:10.1016/j.energy.2022.126026.

[39] Zare, P., Perera, N., Lahr, J., & Hasan, R. (2024). A novel thermal management system for cylindrical lithium-ion batteries using internal-external fin-enhanced phase change material. Applied Thermal Engineering, 238, 121985. doi:10.1016/j.applthermaleng.2023.121985.

[40] Khan, A., Ali, M., Yaqub, S., Khalid, H. A., Khan, R. R. U., Mushtaq, K., Nazir, H., & Said, Z. (2024). Hybrid thermal management of Li-ion battery pack: An experimental study with eutectic PCM-embedded heat transfer fluid. Journal of Energy Storage, 77, 109929. doi:10.1016/j.est.2023.109929.

[41] Alzwayi, A., & Paul, M. C. (2024). Heat transfer enhancement of a lithium-ion battery cell using vertical and spiral cooling fins. Thermal Science and Engineering Progress, 47, 102304. doi:10.1016/j.tsep.2023.102304.

[42] Chen, K., Zhang, Z., Wu, B., Song, M., & Wu, X. (2024). An air-cooled system with a control strategy for efficient battery thermal management. Applied Thermal Engineering, 236, 121578. doi:10.1016/j.applthermaleng.2023.121578.

[43] Fini, A. S., & Gharehghani, A. (2024). Experimental investigation of pressure effect on the PCM performance in Li-ion battery thermal management system. Journal of Energy Storage, 79, 110273. doi:10.1016/j.est.2023.110273.

[44] Shen, X., Cai, T., He, C., Yang, Y., & Chen, M. (2023). Thermal analysis of modified Z-shaped air-cooled battery thermal management system for electric vehicles. Journal of Energy Storage, 58. doi:10.1016/j.est.2022.106356.

[45] Oyewola, O. M., & Idowu, E. T. (2024). Effects of step-like plenum, flow pattern and inlet flow regime on thermal management system. Applied Thermal Engineering, 243, 122637. doi:10.1016/j.applthermaleng.2024.122637.

[46] Tian, Z., Huang, Z., Zhou, Y., Cao, Z., & Gao, W. (2024). Design and experimental study on wave-type microchannel cooling plates for marine large-capacity battery thermal management. Applied Thermal Engineering, 236, 121571. doi:10.1016/j.applthermaleng.2023.121571.

[47] Weragoda, D. M., Tian, G., Cai, Q., Zhang, T., Hing Lo, K., & Gao, Y. (2024). Conceptualization of a novel battery thermal management system based on capillary-driven evaporative cooling. Thermal Science and Engineering Progress, 47, 102320. doi:10.1016/j.tsep.2023.102320.

[48] Oyewola, O. M., Awonusi, A. A., & Ismail, O. S. (2023). Design optimization of Air-Cooled Li-ion battery thermal management system with Step-like divergence plenum for electric vehicles. Alexandria Engineering Journal, 71, 631–644. doi:10.1016/j.aej.2023.03.089.

[49] Li, W., Xiao, M., Peng, X., Garg, A., & Gao, L. (2019). A surrogate thermal modeling and parametric optimization of battery pack with air cooling for EVs. Applied Thermal Engineering, 147, 90–100. doi:10.1016/j.applthermaleng.2018.10.060.